THE JOURNAL OF PHYSICAL CHEMISTRY A

Article

Cite This: J. Phys. Chem. A 2019, 123, 1100−1109

pubs.acs.org/JPCA

Shedding Light on the Dark Corners of Metal−Organic Framework Thin Films: Growth and Structural Stability of ZIF-8 Layers Probed by Optical Waveguide Spectroscopy

Juan A. Allegretto,[†,‡] Jakub Dostalek,[§] Matías Rafti,[†] Bernhard Menges,[∥] Omar Azzaroni,[*,†] and Wolfgang Knoll[⊥,#]

[†]Instituto de Investigaciones Fisicoquímicas Teóricas y Aplicadas (INIFTA), Departamento de Química, Facultad de Ciencias Exactas, Universidad Nacional de La Plata, CONICET, Calle 64 y Diag. 113, 1900 La Plata, Argentina

[‡]Universidad Nacional de San Martin (UNSAM), San Martín, Argentina

[§]Biosensor Technologies, AIT-Austrian Institute of Technology GmbH, Konrad-Lorenz-Strasse 24, 3430 Tulln, Austria

[∥]Resonant Technologies GmbH, Bahnhofstraße 70, 55234 Framersheim, Germany

[⊥]Competence Center for Electrochemical Surface Technology, Konrad Lorenz Strasse 24, 3430 Tulln, Austria

[#]AIT Austrian Institute of Technology, Giefinggasse 4, 1210 Vienna, Austria

Supporting Information

ABSTRACT: Metal−organic framework (MOF) thin films are promising materials for multiple technological applications, such as chemical sensing. However, one potential limitation for their widespread use in different settings is their stability in aqueous environments. In the case of ZIF-8 (zeolitic imidazolate framework) thin films, their stability in aqueous media is currently a matter of debate. Here, we show that optical waveguide spectroscopy (OWS), in combination with surface plasmon resonance (SPR) spectroscopy, offers a convenient way for answering intriguing questions related to the stability of MOF thin films in aqueous solutions and, eventually provide a tool for assessing changes in MOF layers under different environmental conditions. Our experiments relied on the use of ZIF-8 thin films grown on surface-modified gold substrates, as optical waveguides. We have found a linear thickness increase after each growing cycle and observed that the growing characteristics are strongly influenced by the nature of the primer layer. One of our findings is that substrate surface modification with a 3-mercapto-1-propanesulfonate (MPSA) primer layer is critical to achieve ZIF-8 layers that can effectively act as optical waveguides. We observed that ZIF-8 films are structurally stable upon exposure to pure water and 50 mM NaCl solutions but they exhibit a slight swelling and an increase in porosity probably due to the permeation of the solvent in the intergrain mesoporous cavities. However, OWS revealed that exposure of ZIF-8 thin films to phosphate-buffered saline solutions (pH 8) promotes significant film degradation. This poses an important question as to the prospective use of ZIF-8 materials in biologically relevant applications. In addition, it was demonstrated that postsynthetic polyelectrolyte modification of ZIF-8 films has no detrimental effects on the structural stability of the films

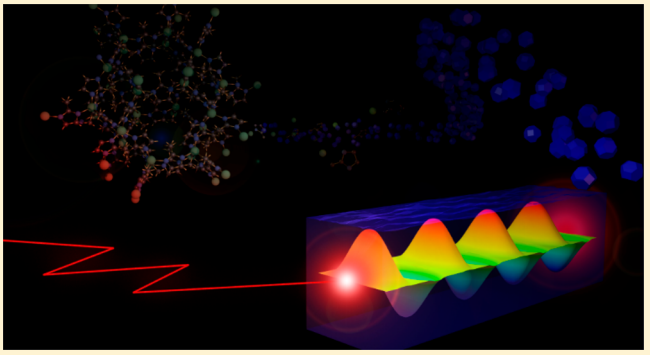

INTRODUCTION

Metal−organic frameworks (MOFs)[1,2] can be defined as infinite porous coordination networks constituted by noncovalently linked organic and inorganic units and offer numerous attractive properties including high surface area, chemical versatility, and relatively high chemical and thermal stability. Owing to these features, MOFs have been used to pursue a wide range of applications, to name a few, gas sensors,[3] adsorbents for liquid- and gas-phase separations,[4] supports for drug-delivery systems,[5] or separation membranes.[6] Moreover, the facile synthesis methods and versatility regarding structural and surface chemistry fine-tuning via either pre- or postsynthetic procedures[7,8] add additional appeal to the integration of MOFs in catalytic and adsorption-related mixed platforms.[9−11] This relatively new class of materials can be used to prepare films using different strategies depending on the targeted application; e.g., direct spin-coating using colloidal dispersions of nano/microcrystals generates thick and eminently nonsmooth films, while surface-mounted MOF quasi-monolayer thin films (SURMOFs) allow for the

Received: October 1, 2018
Revised: November 11, 2018
Published: November 19, 2018

DOI: 10.1021/acs.jpca.8b09610
J. Phys. Chem. A 2019, 123, 1100−1109

observation of nonbulk physical and chemical properties.[12−14] SURMOFs can be synthesized via the Langmuir−Blodgett method, or directly on top of substrates exposing suitable moieties that would act as primers for growth enhancement. It was also previously demonstrated that postsynthetic modification of porous films (not only for MOF growth but also, in general; e.g., for mesoporous silica) using polyelectrolytes can yield a pH-responsive material or can allow modulation of polar character.[15−19]

An extensively used MOF is the so-called ZIF-8 (zeolitic imidazolate framework, available commercially as BASF-BASOLITE-Z1200), which features a sodalite-like crystalline microporous network based on Zn^{2+} clusters tetrahedrally coordinated by 2-methylimidazolate ions (mIm^-). ZIF-8 was successfully employed for separations,[20−22] in mixed membranes,[23−25] and even for the synthesis of hybrid membranes.[26−29] There are many different strategies for synthesizing ZIF-8 films, but the hydro/solvothermal method remains the most popular, in terms of both simplicity and reproducibility. One of the areas in which the use of MOFs, in general, and ZIF-8, in particular, is gaining increasing interest is sensor technologies,[30−32] which takes advantage of their high microporosity and surface area. A recent example of ZIF-8 film use for sensing applications is the work of Lu and Hupp,[33] in which the authors took advantage of the effect of different adsorbed analytes on the Fabry−Pérot interference phenomena (which gives rise to different colors) in order to detect such chemicals via UV−vis transmission spectroscopy. Propane, ethanol, water, and water/ethanol mixtures were used by taking in consideration the hydrophobicity of ZIF-8 micropores. In a similar fashion, Li et al. presented a photonic crystal fabricated with a structured ZIF-8 thin layer with narrow spectral resonances.[34] Time-resolved reflectometry performed on this material allowed for the monitoring of acetonitrile adsorption in the ZIF-8 layer. Another possible strategy is to probe the interaction between analyte and MOF indirectly with an external optical element. This strategy was followed by Tao et al., who used a ZIF-8-coated micro ring resonator (MRR). Detection of volatile organic compounds (VOCs) such as methanol, propylene, and benzene at concentration levels as low as ppb was reported on the basis of the induced refractive index (RI) changes, which detune the MRR resonant wavelengths.[35] In a similar way, Kim et al. used a ZIF-8-coated optical fiber for monitoring a selected gas-phase analyte.[36] Chocarro-Ruiz et al. recently developed an interferometric CO_2 sensor using a multilayer architecture that includes a Si_3N_4 waveguide coated with an adsorbing ZIF-8 nanocrystals layer, and a final protective polydimethylsiloxane (PDMS) coating. Detection limits of such a sensor are 3130 ppm at room temperature and 774 ppm at room temperature.[37]

MOF stability toward aqueous solutions or gases/water vapor mixtures is a matter of great importance[38−42] in order to harness their potential in practical applications. However, the literature shows that MOFs present different degrees of stability in aqueous media[43] and it is currently a matter of debate. For example, XRD analysis showed that ZIF-8 colloidal dispersions remain stable at room temperature and in boiling water, even for 7 days.[44,45] Contrary to these observations, Zhang et al. showed that thin α-alumina supported ZIF-8 membranes are not stable toward water exposure and highly dependent on the pH value.[41] These examples show that characterization of both surface and bulk properties is necessary to address MOFs' stability in a definitive way.

Optical waveguide spectroscopy (OWS) technique and the close-related surface plasmon resonance (SPR) spectroscopy offer a convenient way for answering the above-discussed questions and eventually provide a tool for assessing changes in MOF layers exposed to different conditions. One of the earliest examples of the use of SPR and OWS for characterization of functional materials was given by Knoll.[46] Of course, each specific material acting as waveguide would bring new specific features for analyte detection or stimuli-responsive behavior. The review presented by Ma et al.[47] provides a compilation of a great variety of polymeric materials used as waveguides that can act as probes for many processes occurring inside nanoporous materials (see, e.g., refs 48 and 49), characterization of block copolymers in thin films,[50] detection of structural changes on such films after exposure to different physical and chemical stimuli,[51] and variations on lateral film structure due nanoparticle incorporation.[52]

Synthesizing porous crystalline materials such as MOFs with the capability of acting as waveguides opens the path not only for sensing applications but also for the observation of their structural stability. The synthesis of lanthanide-based MOFs capable of acting as waveguides has been reported already by Yang et al.[53] Considering the physical characteristics required for a material to be used as an optical waveguide,[47] and the typical properties and morphologies reported for MOF films and membranes,[54] it might look like a difficult task to bring these two worlds together. However, Hou et al. showed that it is possible to achieve sufficiently uniform ZIF-8 films by a method that can be classified as liquid-phase epitaxial growth, taking advantage of appropriate surface-anchoring moieties.[55]

We hereby report the use of ZIF-8 MOF films as optical waveguides for the first time to the best of our knowledge. ZIF-8 optical waveguides were constructed on surface-modified gold substrates, in order to characterize film growth process and to determine structural stability toward the exposure to different aqueous environments. The suitability of this approach to elucidate the interaction of ZIF-8 films with modifying agents such as polyelectrolyte solutions (postsynthetic modification allows for the application of many different fine-tuning steps in terms of material's structure-response as recently reported)[19,56] is demonstrated. In conjunction with effective medium theory, the optical response of ZIF-8 films can be quantified in terms of thickness, surface mass density, and porosity variations, which are of the utmost importance for any sensor-related application.

EXPERIMENTAL SECTION

Chemicals. Sulfuric acid, zinc nitrate hexahydrate ($Zn(NO_3)_2{\cdot}6H_2O$, or ZnN), 2-methylimidazole (or HmIm), 3-mercapto-1-propanesulfonic acid sodium salt (MPSA), 70 kDa poly(4-styrenesulfonic acid sodium salt) (NaPSS), anhydrous methanol, sodium chloride, sodium phosphate monobasic monohydrate ($NaH_2PO_4{\cdot}H_2O$), and sodium phosphate dibasic dihydrate ($Na_2HPO_4{\cdot}2H_2O$) were purchased from Sigma-Aldrich and used without further purification. Ultrapure Milli-Q water (18.24 MΩ cm) was used for all the aqueous solutions and washing steps. Further details on the solutions used can be found in the Supporting Information.

Optical setup. A HeNe laser beam (2 mW, λ = 632.8 nm) was coupled to a right-angle LASFN9 glass prism in an SPR spectrometer instrument, operated in the Kretschmann

DOI: 10.1021/acs.jpca.8b09610
J. Phys. Chem. A 2019, 123, 1100−1109

Scheme 1. Schematics of (a) ZIF-8 Film Growth, (b)-i *in-Situ* Probing of 5*x*-ZIF-8 Films in Aqueous Environments, and (b)-ii *in-Situ* Probing of Polyelectrolyte Infiltration on 5*x*-ZIF-8 Films

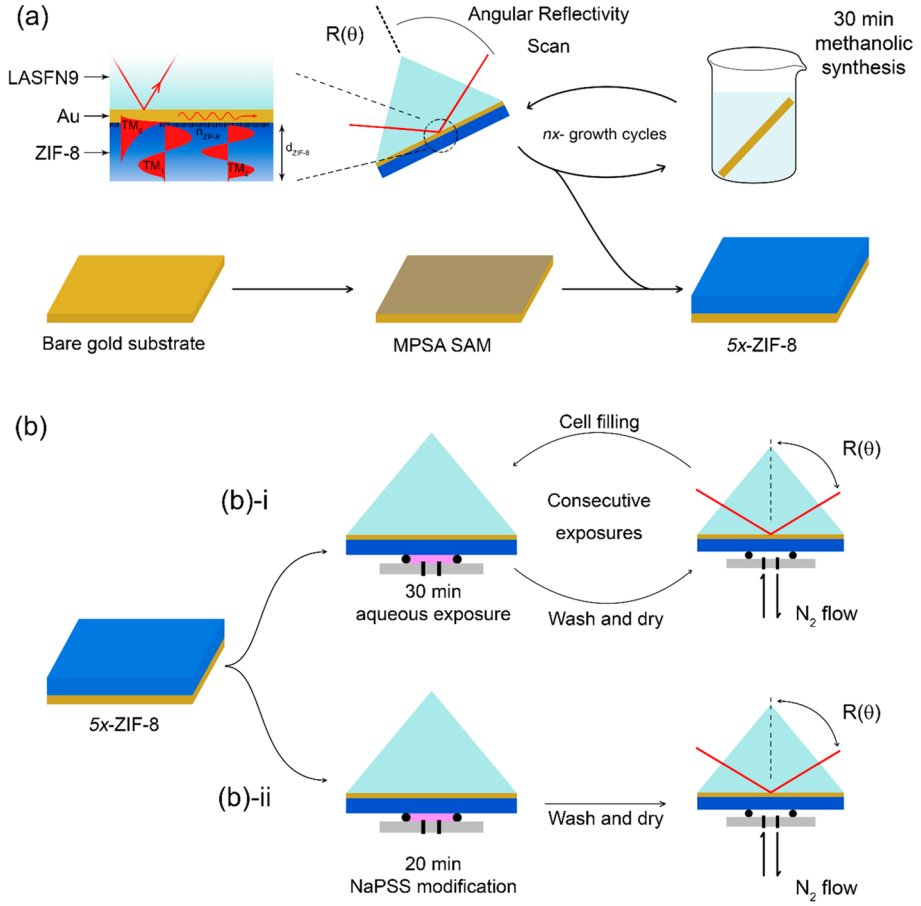

configuration; see Scheme S1. The ZIF-8 layers were grown on a LASFN9 glass substrate that was optically matched to the prism base by using immersion oil. All measurements were carried out under N_2 flow over the ZIF-8 waveguide surface by using a flow cell that was clamped at the prism base. The angle of incidence θ of the laser beam incident on the ZIF-8 surface was controlled by a rotation stage (from Huber) and its polarization was set by a Glan-Thompson polarizer as transverse electric (TE) or transverse magnetic (TM). The intensity of the laser beam reflected at the prism base with a ZIF-8 waveguide film was recorded by a photodiode detector connected to a lock-in amplifier as a function of incidence angle $R(\theta)$. WINSPALL software (version 3.02, Max Planck Institute for Polymer Research) was used to fit the experimental data $R(\theta)$, based on Fresnel equations. In the fitting protocol, we assumed a single and isotropic layer that represents the ZIF-8 waveguide layer on top of the Cr and Au layers (see Supporting Information file, Table S1).

Synthesis of ZIF-8 Films. Initially, the glass substrates were washed via subsequent 15 min ultrasonication steps: 1% Hellmanex III solution, pure water, and ethanol. Then 50 nm thick gold layer was prepared by thermal sputtering using a UNIVEX 450C apparatus (Leybold) on top of a LASFN9 glass substrate with a 2 nm Cr adhesion-promoting layer. ZIF-8 thin films were synthesized on the top of the gold surface according to previously reported protocols.[19] Briefly, a gold-coated substrate was placed overnight in MPSA aqueous solution. Then, the substrate was washed with Milli-Q pure water and dried under a stream of N_2. The gold substrate with the MPSA self-assembled monolayer (SAM) exposing sulfonate moieties was placed vertically in a 25 mM ZnN solution prepared in anhydrous methanol, and then, an equal volume of 50 mM HmIm solution (also prepared in anhydrous methanol) was added. After 30 min, the substrate was washed generously with anhydrous methanol and dried under a N_2 stream. This sequence represents a single "growth cycle". By repeating these growth cycles, it is possible to control the thickness of the formed ZIF-8 film in a stepwise manner (see Scheme 1a). The films prepared in such way will be referred to as *nx*-ZIF-8, where *n* indicates the number of growth cycles used.

***In-Situ* Probing in Aqueous Environment.** For *in situ* experiments, a ~10 μL flow cell was mounted on top of the ZIF-8 layer surface. The cell was composed of a rubber O-ring pressed against the ZIF-8 surface by an acrylic slide with inlet and outlet ports connected to tubing with a diameter of 0.8 mm. The flow cell was filled with the tested solution, and after the elapsed exposure time (30 min) in static conditions, the solution was removed from the flow cell by using a syringe, subsequently rinsed with water, and completely dried with N_2 flow for 30 min (see Scheme 1b-i). The N_2 flow was kept during the angular reflectivity scan $R(\theta)$.

***In-Situ* Probing of Polyelectrolyte Infiltration.** Modification with the NaPSS solution was carried *in situ*, similar to the exposure to the exposure to aqueous environments above-mentioned: the polyelectrolyte solution was injected into the flow cell for 20 min and then the surface was washed with

DOI: 10.1021/acs.jpca.8b09610
J. Phys. Chem. A 2019, 123, 1100−1109

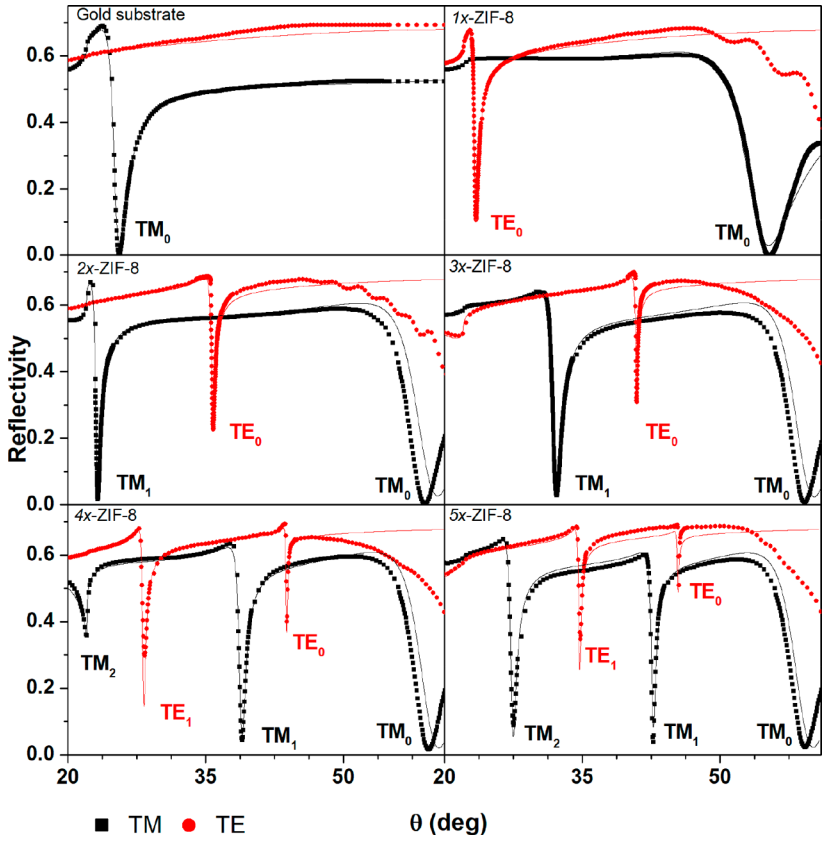

Figure 1. Cycle-by-cycle progression of the resonant coupling of guided modes under TM (black squares) and TE (red circles) polarization, and model fitting (full lines) for the 5*x*-ZIF-8 film construction.

water and dried in N_2 (see Scheme 1b-ii). The film treated this way will be hereafter referred as *nx*-ZIF-8+PSS.

RESULTS AND DISCUSSION

Films Growth and Properties. First, ZIF-8 film growth was optically characterized using resonantly excited waveguide modes. As Figure 1 shows, this excitation is manifested as a series of dips in the angular reflectivity spectrum $R(\theta)$ in both TM and TE polarization, which change positions after each growth cycle. The waveguide modes supported by ZIF-8 films arise from the total internal reflection of light at the outer film interface and from the reflection at the inner gold surface. Depending on the thickness $d_{ZIF\text{-}8}$ and the refractive index $n_{ZIF\text{-}8}$ of the film, multiple guided waves referred to as TM_m or TE_m (m is the number of nodes of that particular field distribution) can be excited with the optical beam launched into the prism and hitting the layer structure (see Scheme 1a). The excitation of guided waves is resonant and occurs only at specific angles (θ), at which the laser beam is phase-matched with TM_m or TE_m modes traveling along the surface.

The synthesis of the ZIF-8 film was characterized by performing angular reflectivity spectra $R(\theta)$ measurements after each growth cycle. As can be seen in Figure 1, $R(\theta)$ prior to the ZIF-8 first growth cycle shows one resonance in the TM polarization (TM_0 mode corresponding to surface plasmon (SP) at the gold/air interface) and no resonance in TE polarization. After the first cycle of ZIF-8 growth, the resonant angle at which the SP is excited shifts by almost 30° and the excitation of the first guided mode TE_0 occurs in TE polarization. With the subsequent growth cycles (nx = 2x, 3x, ..., 5x), the SP angular position does not change significantly, the TE_0 guided mode shifts to higher angular values, and additional higher order guided modes in both TM and TE polarizations, respectively, occur. After the complete film synthesis (five growth cycles), TM_0 (SP) and four guided modes $TE_{0,1}$ and $TM_{1,2}$ are observed. The measured reflectivity curves $R(\theta)$ have been fitted with a Fresnel reflectivity-based model in order to determine changes in the thickness $d_{ZIF\text{-}8}$ and refractive index $n_{ZIF\text{-}8}$ of the synthesized ZIF-8 films. For the first growth cycle, the fitting of two observed resonances due to SP and TE_0 modes, allows for determination of both $d_{ZIF\text{-}8} = 174 \pm 4$ nm and $n_{ZIF\text{-}8} = 1.357 \pm 0.005$ parameters. For the films obtained after subsequent growth cycles (nx = 2x to 5x), fitting all the observed resonances becomes not possible using the model, and the experimental SP angular position exhibits a slight deviation (between 1° and 1.3°) with respect to the fit. This difference can be attributed to the fact that the probing distance of the SP is only around 100 nm from the gold surface, and thus it only partially overlaps with the first layer and it does not allow for probing of the increased thickness gained after additional synthesis steps. On the contrary, the guided modes $TM_{1,2}$ and $TE_{0,1}$ exhibit a more delocalized profile of electromagnetic field and thus probe the entire thickness of ZIF-8 layer. These discrepancies indicate that effective optical properties of ZIF-8 films at the very interface with the gold surface (as observed via SP mode variations) may be slightly different from those values obtained from thickness-averaged determinations when the entire structure is probed (as observed by $TM_{1,2}$ and $TE_{0,1}$). Further discussion addressing this point will be given, together with the MPSA monolayer effect (see below).

DOI: 10.1021/acs.jpca.8b09610
J. Phys. Chem. A 2019, 123, 1100−1109

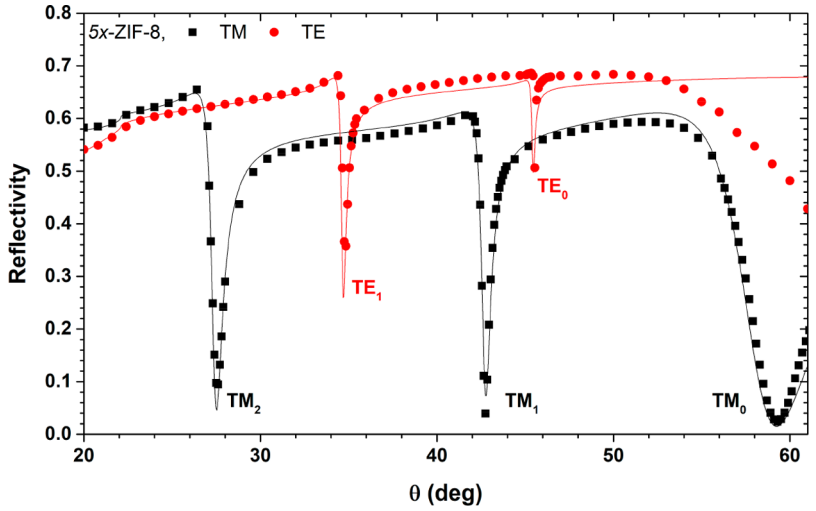

Figure 2. Resonant coupling for the 5*x*-ZIF-8 film under TM (black squares) and TE (red circles) polarization. Experimental points were fitted with a bilayer model (full line).

It is possible to tackle the problem of the observed difference between the experimental and fitted curves for the SP angular position by adopting a slightly more complex bilayer model. Under this approach, the first layer would have the thickness found for the 1*x*-ZIF-8 films, while the thickness of the second layer will change according to the increasing number of growth cycles (total thickness would be the sum of both assumed layers). Regarding the refractive index (RI), the values would change for each layer, in order to correctly fit the experimental curves. Figure 2 shows as an example of how the two-layer model describes accurately the SP resonant angular position as well as all the guided modes.

Although there is better agreement between experiments and fittings with this two-layer model, the parameters obtained are quite similar to what is obtained using the much simpler one-layer model; e.g., thickness progression was found to be exactly the same (138 ± 3 nm/cycle). However, the two-layer model results in a RI value for the first layer which is lower than the RI obtained for the second layer. Moreover, having in mind that film porosity should only depend on its crystalline structure, one can safely disregard the two-layer model, since the porous fraction was found to be larger for the first layer than for the second layer after applying Bruggeman's theory. Additionally, structural stability of ZIF-8 film after post-synthetic modifications (see below) can be better understood by assuming the existence of a single unit rather than a two-layer structure. On the basis of the above discussion, we selected the one-layer model for describing the observed behavior.

The parameters $d_{ZIF\text{-}8}$ and $n_{ZIF\text{-}8}$ were determined for each subsequent growth cycle, as presented in the Supporting Information (Table S2). Evolution of film thickness is shown in Figure 3. These experiments reveal a linear increase in the thickness per growth cycle with a slope of 138 ± 3 nm/cycle. The standard deviation in thickness of about 2% indicates a highly reproducible synthesis process as determined by comparing four equivalent 5*x*-ZIF-8 films, each of which was measured and fitted on three different spots. From this analysis, it was also possible to calculate an average real part of the refractive index of ZIF-8: $\mathrm{Re}\{n_{ZIF\text{-}8}\} = 1.352 \pm 0.004$ at λ = 632.8 nm, in good agreement with previously reported values.[42] Using the Bruggeman's effective medium theory

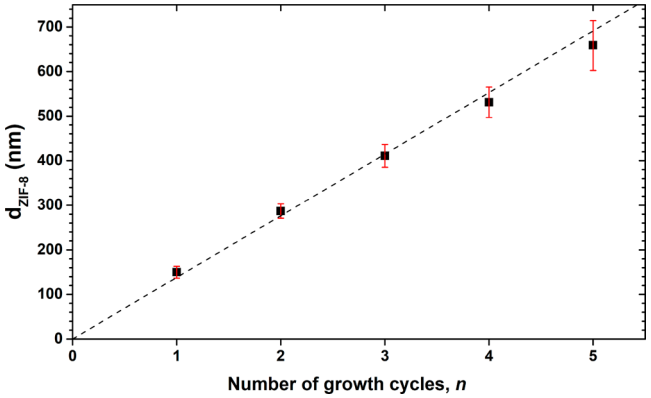

Figure 3. Thickness evolution ($d_{ZIF\text{-}8}$) upon sequential synthesis of 5*x*-ZIF-8 films. Each value was averaged from measurements on four different samples and three distinct spots. Error bars correspond to standard errors and the dashed line represents the linear fit (r^2 = 0.998) of the measured values.

(calculation details can be found in the Supporting Information) a porous fraction of 0.6 was determined for all prepared 5*x*-ZIF-8 films. This result is in line with previously reported porosity values for similar ZIF-8 crystals (58.8%).[57]

Note that the Bruggeman approximation assumes that the refractive index of the pores is 1, which is accurate if the pores are completely empty, i.e., free from residual solvent. If we consider that the refractive indexes as obtained from OWS fittings are in good agreement with the available reported values in the literature for pure ZIF-8 material and the refractive index of methanol is 1.3263, then we can assume that the presence of residual solvent trapped in the pores is negligible because the effect of having a considerable amount of residual methanol in the pores would result in much higher RI values, which is not the case.

Interestingly, the observed growth rate of 138 ± 3 nm/cycle is significantly higher than what previously reported in the literature (~70 nm/cycle).[55] This difference can be ascribed to the effect of sulfonate moieties introduced to the gold interface by the MPSA SAM primer.[58,59] These anchoring moieties are crucial for obtaining a homogeneous ZIF-8 layer that can serve as an efficient slab waveguide. For comparison, Figure S1 (see

DOI: 10.1021/acs.jpca.8b09610
J. Phys. Chem. A 2019, 123, 1100−1109

Supporting Information) shows the progression of the angular reflectivity scans $R(\theta)$ for the growth of ZIF-8 at bare gold surfaces, i.e., without MPSA. The experiment reveals that the angular width of the TM_0 (SP) resonance is significantly broader and that higher waveguide modes are not apparent. This can be ascribed to the strongly deteriorated lateral homogeneity of the ZIF-8 film, which can be quantified by the use of the effective extinction coefficient κ of the ZIF-8 layer (imaginary part of the refractive index $\mathrm{Im}\{n_{\mathrm{ZIF\text{-}8}}\}$). This parameter can be determined by the fitting analysis of $R(\theta)$ and increasing κ is typically associated with a broadening of the observed dips in $R(\theta)$. The effective extinction coefficient κ takes into account scattering on defects with a size comparable to or higher than the used wavelength λ and it is important to note neither Zn^{2+} nor mIm^- (which is used to synthesize the ZIF-8 films) exhibits absorption at selected wavelength λ.

Table 1 provides the comparison of thickness $d_{\mathrm{ZIF\text{-}8}}$ and extinction coefficient κ determined for the films prepared on a gold surface without and with an MPSA SAM. MPSA was expected to promote heterogeneous nucleation of ZIF-8 on the surface triggered by precoordination of Zn^{2+} ions by the surface-exposed sulfonate moieties.[59] There were two main results supporting the assumption above. First, the thickness value $d_{\mathrm{ZIF\text{-}8}}$ for the 1x-ZIF-8 is almost 20 times higher with MPSA anchoring, but for the next growth cycles these differences start to decrease, and at the end, 5x-ZIF-8 synthesized on an MPSA SAM is only 1.5 times greater than when no MPSA SAM is present. Second, the extinction coefficient κ of films prepared on MPSA SAM is at least 1 order of magnitude lower than that without this anchoring layer. In other words, by providing these initial nucleation points distributed across the gold surface, a higher density of (probably smaller) nuclei is achieved, and ultimately causes a much more homogeneous film compared to what is obtained when nucleation occurs preferentially in the homogeneous phase and nanocrystals thus formed start to aggregate to form the film. The fact that the extinction coefficient κ decreases with film growth progression over MPSA SAM also supports the hypothesis, as each growth cycle is influenced by the presence of the previously synthesized ZIF-8 layer. The above interpretation brings further support for the use of a single layer model to describe the system; i.e., each growth cycle does not generate layers with different morphology but rather contributes to a one-block structure with increasing thickness.

Table 1. Comparison of Thickness ($d_{\mathrm{ZIF\text{-}8}}$) and Extinction Coefficient (κ) for 5x-ZIF-8 Films Synthesized on a Gold Surface with and without an MPSA Nucleation Layer

	thickness $d_{\mathrm{ZIF\text{-}8}}$ (nm)		ratio	ext coefficient κ		ratio
growth cycle (nx)	with MPSA	without MPSA	d_{wo}/d_w	with MPSA	without MPSA	κ_{wo}/κ_w
1	150	8.8	0.06	0.0035	0.312	89
2	287	39	0.14	0.0030	0.276	92
3	410	91	0.22	0.0016	0.150	94
4	530	359	0.68	0.0017	0.049	29
5	658	426	0.65	0.0017	0.036	21

Structural Stability of ZIF-8 Films in Aqueous Environment. The stability of the ZIF-8 film is crucial for determining its possible applications. A useful quantity to evaluate this feature is the layer surface mass density Γ, which takes into account the potential loss in the porous material due to etching caused by exposure to different solvents. Surface mass density can be shown to be proportional to the term $d_{\mathrm{ZIF\text{-}8}}(1 - f_{\mathrm{pores}})$, where the volume fraction of pores f_{pores} can be obtained from fitted $\mathrm{Re}\{n_{\mathrm{ZIF\text{-}8}}\}$ by the Bruggeman effective medium theory (see Supporting Information).

In order to study the stability of synthesized materials, 5x-ZIF-8 films were investigated after they were exposed to Milli-Q water, NaCl 50 mM aqueous solution, and finally to 10 mM PBS, pH = 8, aqueous buffer. NaCl was chosen in order to regulate ionic strength because Na^+ and Cl^- ions were proved to have no effect on the crystalline structure of ZIF-8.[60,61] Figure 4 shows the relative changes between final and initial thicknesses as $(d^{f}_{\mathrm{ZIF\text{-}8}} - d^{i}_{\mathrm{ZIF\text{-}8}})/d^{i}_{\mathrm{ZIF\text{-}8}}$ (top), and the relative changes between final and initial Γ as $(\Gamma_f - \Gamma_i)/\Gamma_i$ (bottom) after sequential (30 min) static exposure to each of the above solutions. Results obtained reveal that films exposed to Milli-Q water and NaCl experiment some swelling; a 15% thickness increase was detected compared to what is observed for freshly prepared films after five exposure cycles (equivalent to 150 min). Such swelling is accompanied by a decrease in surface mass density Γ, which reaches a 20% loss of ZIF-8 mass after five exposures (see Table S3 for the further details). Interestingly, ZIF-8 films were found to behave dramatically differently in PBS solution. The film underwent an initial thickness increase by 12% after 30 min exposure of PBS followed by a gradual decrease to a final value of 50% after five exposure cycles. In addition, Γ shows a continuous decrease until a loss of almost 65%.

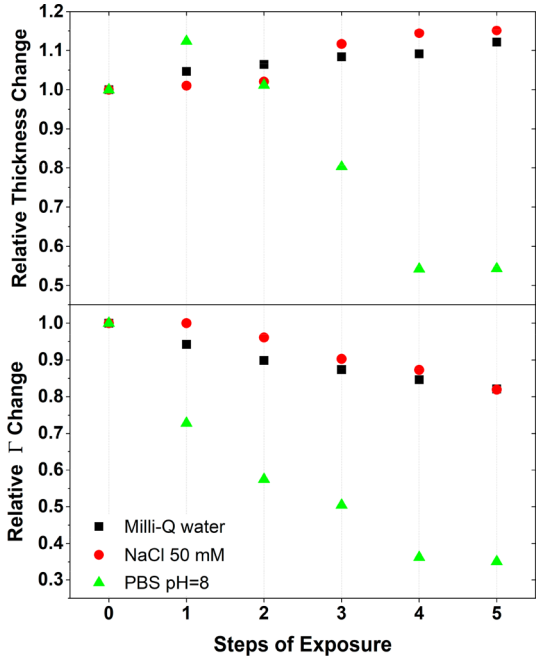

Figure 4. Relative changes on thickness (top) and Γ (bottom) for 5x-ZIF-8 films after five consecutive 30 min exposures to Milli-Q water (black squares), 50 mM NaCl (red circles), and 10 mM PBS, pH = 8 (green triangles).

The observed changes in Γ can be ascribed to variations in the thickness as well as in the porous fraction, f_{pores}. Figure 5 provides this information, which confirms that ZIF-8 films gradually undergo an irreversible swelling together with a release of occluded material when exposed to Milli-Q and NaCl 50 mM solution. Contrary to these experiments, the

DOI: 10.1021/acs.jpca.8b09610
J. Phys. Chem. A 2019, 123, 1100−1109

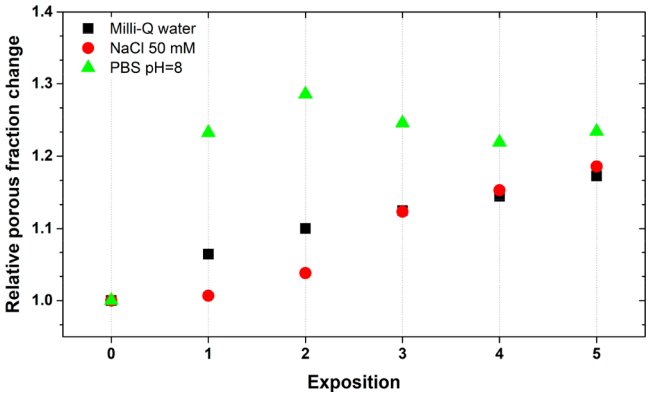

Figure 5. Relative porous fraction change for 5*x*-ZIF-8 films after five consecutive exposures to Milli-Q water (black squares), 50 mM NaCl (red circles), and 10 mM PBS, pH = 8 (green triangles).

porous fraction f_{pores} abruptly increases by 20% after the first exposure to phosphate-buffered saline (PBS) solution (pH 7.4) and afterward it does not change substantially. These observations indicate that, after exposure to Milli-Q water and 50 mM NaCl solution, the film slowly swells and the porosity f_{pores} increases. However, exposure to PBS causes the film to experience an initial thickness increase followed by a gradual material loss without collapsing, which decreases its thickness although porosity shows no variation. It is worth mentioning that Wang et al. already reported such an effect for ZIF-8 exposed to PBS solutions[60] but higher pH values were used (9.0 and 13.2), for which the material is not expected to be stable toward hydrolysis. Additionally, in the same reported work, higher concentrations were used, which translates to almost 100 mM ionic strength and means that no direct comparison is possible to the results hereby presented.

These results reveal that the exposure of ZIF-8 thin films to phosphate-buffered saline solutions results in the film degradation. The degradation mechanism is not clear but according to our OWS data we can rule out the formation of new solid phases arising from the reaction of Zn^{2+} and phosphate. Zinc phosphate phases exhibit refractive indexes between 1.5 and 1.7, depending on its nature. As shown in the Supporting Information, Table S3, the refractive index of the ZIF-8 layer is lower after each PBS exposure. In addition, its thickness and surface mass density decrease in the same fashion. These two pieces of information point toward a dissolution effect caused by PBS exposure of the ZIF-8 layer, rather than a substitution for zinc to yield a phosphate phase. Also, the porous fraction of the ZIF-8 layer increases after each exposure; again, if any zinc−phosphate phase would be growing, since it features no porosity, the observed porous fraction should decrease, and this has not been observed in our experiments.

Polyelectrolyte/ZIF-8 Interaction. It was previously reported that PSS can modify the polar character of intergrain mesoporous cavities in ZIF-8 films, which in turn, alters effective diffusion coefficients of the probe molecules going through the film.[19] This opens the path for the use of the diffusion−reaction approach for the synthesis of film-embedded metal nanoparticles. The successful polyelectrolyte capping of films constituted by porous materials depends on the nature and strength of the interactions between capping agent and the pore walls. Possible architectures obtained are either confined (the polyelectrolyte remains segregated on a different phase causing no effect on the porous material) or segregated (the polyelectrolyte percolates the entire porous structure causing a change on the overall films' polar character). In order to gain insight into the outcome of such processes, a series of OWS measurements were carried out on films that were exposed to PSS polymer solutions (PSS was selected due to both its anionic nature and its affinity toward Zn^{2+} moieties on ZIF-8). Figure 6 shows a comparison of

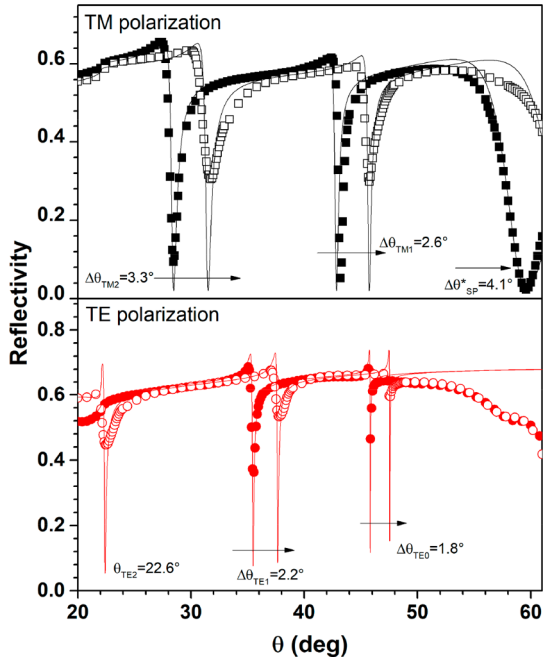

Figure 6. Resonant coupling of guided modes under TM (black squares, top) and TE (red circles, bottom) polarization for a 5*x*-ZIF-8 film (filled dots) and 5*x*-ZIF-8+PSS film (empty dots). *Determined by considering the fitted-SP angular position.

reflectivity curves $R(\theta)$ before (5*x*-ZIF-8) and after modification with PSS (5*x*-ZIF-8+PSS). These curves reveal that the angles at which the resonant coupling to guided waves occurs are shifted by about 3°. By fitting the experimental data obtained, we determined a (relatively) strong increase in RI from $n_{ZIF\text{-}8}$ = 1.352 to 1.375, together with a small (1.74%) increase of film thickness $d_{ZIF\text{-}8}$. Since the strong refractive index increase relates to a decrease in f_{pores}, it can be assumed that PSS efficiently percolates the entire film. This assumption is supported by the fact that, if the PSS would remain mostly surface-confined, the SP (TM_0) resonance angular position should not change. However, the surface plasmon waves probing the gold/ZIF-8 interface show a distinct angular change, which indicates that PSS was distributed through the whole film (see Supporting Information). Although the experimental data were successfully fitted by using a single and isotropic layer, the observed shifts on the different guided modes allow for hypothesizing that, even though PSS percolates the whole film structure, some lateral gradient concentration of PSS could be expected. By applying effective medium theory, it was possible to calculate the remaining porous fraction after PSS modification and to obtain an estimation of the polymer fraction in the film (see Supporting Information). Briefly, the final composition obtained was 40.9% of ZIF-8 (framework), 55.2% empty pores, and 3.9% of polymer. It is possible to say, thus, that PSS modification does

DOI: 10.1021/acs.jpca.8b09610
J. Phys. Chem. A 2019, 123, 1100−1109

not represent a significant decrease in film porosity, which is a core property when MOFs are considered as sensing platforms.

In this regard, it is important to note that there are two contributions to film porosity: (a) the intrinsic ZIF-8 microporosity, which is determined by its crystalline structure (highly hydrophobic due to methyl moieties of 2-methylimidazole linker projected to the pore windows); (b) the mesoporosity arising from the intergrain space. It is evident that due to the molecular size 70 kDa, PSS chains cannot enter ZIF-8 micropores. Then, it is plausible to assume that PSS chains percolate the film through the intergrain mesoporous spaces.

CONCLUSIONS

Surface plasmon resonance in combination with optical waveguide spectroscopy provided new insight into the growth and structural stability of ZIF-8 films toward exposure to aqueous solutions relevant for a wide range of applications. To this end, we have synthesized for the first time wave-guiding MOF films. We have found a linear thickness increase for film growth cycles and showed how each of those cycles is strongly influenced by the previous step in terms of the chemical identity of the starting layer. The experimental setup used allowed us to confirm that substrate surface modification with MPSA monolayer primer is critical in order to achieve ZIF-8 layers that can effectively act as monomode or multimode slab optical waveguides. We have shown also that ZIF-8 films are structurally stable under Milli-Q water and 50 mM NaCl solutions and that the choice of a proper buffered media needs to be carefully considered (i.e., PBS buffer was shown to be deleterious for film stability in the case of ZIF-8 MOF). In addition., it was demonstrated that polyelectrolyte postsynthetic modification of ZIF-8 films modify their surface properties without detrimental effects on the porosity, thus providing a powerful tool for fine-tuning their transport properties.

ASSOCIATED CONTENT

Supporting Information

The Supporting Information is available free of charge on the ACS Publications website at DOI: 10.1021/acs.jpca.8b09610.

Brief description of OWS-SPR technique, schematic representation of surface plasmon (SP) and guided modes, list of sample theoretical layers used, thickness, refractive index, porous fraction, and Γ data, SP resonance changes, progression diagrams of TM and TE modes, response curves, and schematic representation of the different possible scenarios after ZIF-8 film modification (PDF)

AUTHOR INFORMATION

Corresponding Author

*O. Azzaroni. E-mail: azzaroni@inifta.unlp.edu.ar.

ORCID

Jakub Dostalek: 0000-0002-0431-2170

Matías Rafti: 0000-0003-3393-358X

Omar Azzaroni: 0000-0002-5098-0612

Notes

The authors declare no competing financial interest.

ACKNOWLEDGMENTS

This work was supported by CONICET, ANPCyT (PICT-2010-2554, PICT 2013-0905), the Austrian Institute of Technology GmbH (AIT-CONICET Partner Group, Exp. 4947/11, Res. No. 3911, 28-12-2011), Universidad Nacional de La Plata (UNLP), the Austrian Federal ministry for Transportation, Innovation and Technology (GZ BMVIT-612.166/0001-III/I1/2010), by the FFG within the comet program, and from the governments of Lower and Upper Austria. J.A.A. wants to acknowledge CONICET for his doctoral scholarship and the Biosensor Technologies group for the support and help during his stay at AIT.

REFERENCES

(1) Férey, G. Hybrid Porous Solids: Past, Present, Future. *Chem. Soc. Rev.* **2008**, *37* (1), 191−214.

(2) Furukawa, H.; Cordova, K. E.; O'Keeffe, M.; Yaghi, O. M. The Chemistry and Applications of Metal-Organic Frameworks. *Science* **2013**, *341* (6149), 1230444.

(3) Xiang, S.; Zhou, W.; Gallegos, J. M.; Liu, Y.; Chen, B. Exceptionally High Acetylene Uptake in a Microporous Metal−Organic Framework with Open Metal Sites. *J. Am. Chem. Soc.* **2009**, *131* (34), 12415−12419.

(4) Li, J.-R.; Sculley, J.; Zhou, H.-C. Metal−Organic Frameworks for Separations. *Chem. Rev.* **2012**, *112* (2), 869−932.

(5) Della Rocca, J.; Liu, D.; Lin, W. Nanoscale Metal−Organic Frameworks for Biomedical Imaging and Drug Delivery. *Acc. Chem. Res.* **2011**, *44* (10), 957−968.

(6) Li, J.-R.; Ma, Y.; McCarthy, M. C.; Sculley, J.; Yu, J.; Jeong, H.-K.; Balbuena, P. B.; Zhou, H.-C. Carbon Dioxide Capture-Related Gas Adsorption and Separation in Metal-Organic Frameworks. *Coord. Chem. Rev.* **2011**, *255* (15−16), 1791−1823.

(7) Park, J.; Wang, Z. U.; Sun, L.-B.; Chen, Y.-P.; Zhou, H.-C. Introduction of Functionalized Mesopores to Metal−Organic Frameworks via Metal−Ligand−Fragment Coassembly. *J. Am. Chem. Soc.* **2012**, *134* (49), 20110−20116.

(8) Cohen, S. M. Postsynthetic Methods for the Functionalization of Metal−Organic Frameworks. *Chem. Rev.* **2012**, *112* (2), 970−1000.

(9) Gascon, J.; Corma, A.; Kapteijn, F.; Llabrés i Xamena, F. X. Metal Organic Framework Catalysis: Quo Vadis ? *ACS Catal.* **2014**, *4* (2), 361−378.

(10) Fracaroli, A. M.; Siman, P.; Nagib, D. A.; Suzuki, M.; Furukawa, H.; Toste, F. D.; Yaghi, O. M. Seven Post-Synthetic Covalent Reactions in Tandem Leading to Enzyme-like Complexity within Metal−Organic Framework Crystals. *J. Am. Chem. Soc.* **2016**, *138* (27), 8352−8355.

(11) Wang, C.; Tuninetti, J.; WANG, Z.; Zhang, C.; Ciganda, R.; Salmon, L.; Moya, S.; Ruiz, J.; Astruc, D. Hydrolysis of Ammonia-Borane over Ni/ZIF-8 Nanocatalyst: High Efficiency, Mechanism and Controlled Hydrogen Release. *J. Am. Chem. Soc.* **2017**, *139* (33), 11610−11615.

(12) Shekhah, O. Layer-by-Layer Method for the Synthesis and Growth of Surface Mounted Metal-Organic Frameworks (SURMOFS). *Materials* **2010**, *3* (2), 1302−1315.

(13) Liu, B.; Ma, M.; Zacher, D.; Bétard, A.; Yusenko, K.; Metzler-Nolte, N.; Wöll, C.; Fischer, R. a. Chemistry of SURMOFs: Layer-Selective Installation of Functional Groups and Post-Synthetic Covalent Modification Probed by Fluorescence Microscopy. *J. Am. Chem. Soc.* **2011**, *133* (6), 1734−1737.

(14) Arslan, H. K.; Shekhah, O.; Wohlgemuth, J.; Franzreb, M.; Fischer, R. A.; Wöll, C. High-Throughput Fabrication of Uniform and Homogenous MOF Coatings. *Adv. Funct. Mater.* **2011**, *21* (22), 4228−4231.

(15) Brunsen, A.; Cui, J.; Ceolín, M.; del Campo, A.; Soler-Illia, G. J. A. A.; Azzaroni, O. Light-Activated Gating and Permselectivity in Interfacial Architectures Combining "Caged" Polymer Brushes and Mesoporous Thin Films. *Chem. Commun.* **2012**, *48* (10), 1422−1424.

(16) Andrieu-Brunsen, A.; Micoureau, S.; Tagliazucchi, M.; Szleifer, I.; Azzaroni, O.; Soler-Illia, G. J. A. A. Mesoporous Hybrid Thin Film Membranes with PMETAC@Silica Architectures: Controlling Ionic Gating through the Tuning of Polyelectrolyte Density. *Chem. Mater.* **2015**, *27* (3), 808−821.
(17) Fu, Q.; Rao, G. V. R.; Ista, L. K.; Wu, Y.; Andrzejewski, B. P.; Sklar, L. A.; Ward, T. L.; López, G. P. Control of Molecular Transport Through Stimuli-Responsive Ordered Mesoporous Materials. *Adv. Mater.* **2003**, *15* (15), 1262−1266.
(18) Calvo, A.; Yameen, B.; Williams, F. J.; Azzaroni, O.; Soler-Illia, G. J. A. A. Facile Molecular Design of Hybrid Functional Assemblies with Controllable Transport Properties: Mesoporous Films Meet Polyelectrolyte Brushes. *Chem. Commun.* **2009**, *18*, 2553−2555.
(19) Allegretto, J. A.; Tuninetti, J. S.; Lorenzo, A.; Ceolín, M.; Azzaroni, O.; Rafti, M. Polyelectrolyte Capping As Straightforward Approach toward Manipulation of Diffusive Transport in MOF Films. *Langmuir* **2018**, *34* (1), 425−431.
(20) Zhang, K.; Lively, R. P.; Zhang, C.; Koros, W. J.; Chance, R. R. Investigating the Intrinsic Ethanol/Water Separation Capability of ZIF-8: An Adsorption and Diffusion Study. *J. Phys. Chem. C* **2013**, *117* (14), 7214−7225.
(21) Gee, J. A.; Chung, J.; Nair, S.; Sholl, D. S. Adsorption and Diffusion of Small Alcohols in Zeolitic Imidazolate Frameworks ZIF-8 and ZIF-90. *J. Phys. Chem. C* **2013**, *117* (6), 3169−3176.
(22) Wang, B.; Côté, A. P.; Furukawa, H.; O'Keeffe, M.; Yaghi, O. M.; O'Keeffe, M.; Yaghi, O. M. Colossal Cages in Zeolitic Imidazolate Frameworks as Selective Carbon Dioxide Reservoirs. *Nature* **2008**, *453* (7192), 207−211.
(23) Barankova, E.; Tan, X.; Villalobos, L. F.; Litwiller, E.; Peinemann, K.-V. A Metal Chelating Porous Polymeric Support: The Missing Link for a Defect-Free Metal-Organic Framework Composite Membrane. *Angew. Chem., Int. Ed.* **2017**, *56*, 2965.
(24) Pan, Y.; Liu, W.; Zhao, Y.; Wang, C.; Lai, Z. Improved ZIF-8 Membrane: Effect of Activation Procedure and Determination of Diffusivities of Light Hydrocarbons. *J. Membr. Sci.* **2015**, *493*, 88−96.
(25) Jomekian, A.; Behbahani, R. M.; Mohammadi, T.; Kargari, A. Innovative Layer by Layer and Continuous Growth Methods for Synthesis of ZIF-8 Membrane on Porous Polymeric Support Using Poly(Ether-Block-Amide) as Structure Directing Agent for Gas Separation. *Microporous Mesoporous Mater.* **2016**, *234*, 43−54.
(26) Liu, Y.; Li, S.; Zhang, X.; Liu, H.; Qiu, J.; Li, Y.; Yeung, K. L. New Membrane Architecture: ZnO@ZIF-8 Mixed Matrix Membrane Exhibiting Superb H2 Permselectivity and Excellent Stability. *Inorg. Chem. Commun.* **2014**, *48*, 77−80.
(27) Yang, L.; Wang, Z.; Zhang, J. Zeolite Imidazolate Framework Hybrid Nanofiltration (NF) Membranes with Enhanced Permselectivity for Dye Removal. *J. Membr. Sci.* **2017**, *532*, 76−86.
(28) Marti, A. M.; Wickramanayake, W.; Dahe, G.; Sekizkardes, A.; Bank, T. L.; Hopkinson, D. P.; Venna, S. R. Continuous Flow Processing of ZIF-8 Membranes on Polymeric Porous Hollow Fiber Supports for CO_2 Capture. *ACS Appl. Mater. Interfaces* **2017**, *9* (7), 5678−5682.
(29) Hess, S. C.; Grass, R. N.; Stark, W. J. MOF Channels within Porous Polymer Film: Flexible, Self-Supporting ZIF-8 Polyethersulfone Composite Membrane. *Chem. Mater.* **2016**, *28* (21), 7638−7644.
(30) Demessence, A.; Boissière, C.; Grosso, D.; Horcajada, P.; Serre, C.; Férey, G.; Soler-Illia, G. J. A. A.; Sanchez, C. Adsorption Properties in High Optical Quality NanoZIF-8 Thin Films with Tunable Thickness. *J. Mater. Chem.* **2010**, *20* (36), 7676.
(31) Eslava, S.; Zhang, L.; Esconjauregui, S.; Yang, J.; Vanstreels, K.; Baklanov, M. R.; Saiz, E. Metal-Organic Framework ZIF-8 Films As Low-κ Dielectrics in Microelectronics. *Chem. Mater.* **2013**, *25* (1), 27−33.
(32) Li, W. J.; Gao, S. Y.; Liu, T. F.; Han, L. W.; Lin, Z. J.; Cao, R. In Situ Growth of Metal-Organic Framework Thin Films with Gas Sensing and Molecule Storage Properties. *Langmuir* **2013**, *29* (27), 8657−8664.
(33) Lu, G.; Hupp, J. T. Metal−Organic Frameworks as Sensors: A ZIF-8 Based Fabry−Pérot Device as a Selective Sensor for Chemical Vapors and Gases. *J. Am. Chem. Soc.* **2010**, *132* (23), 7832−7833.
(34) Li, L.; Jiao, X.; Chen, D.; Lotsch, B. V.; Li, C. Facile Fabrication of Ultrathin Metal-Organic Framework-Coated Monolayer Colloidal Crystals for Highly Efficient Vapor Sensing. *Chem. Mater.* **2015**, *27* (22), 7601−7609.
(35) Tao, J.; Wang, X.; Sun, T.; Cai, H.; Wang, Y.; Lin, T.; Fu, D.; Ting, L. L. Y.; Gu, Y.; Zhao, D. Hybrid Photonic Cavity with Metal-Organic Framework Coatings for the Ultra-Sensitive Detection of Volatile Organic Compounds with High Immunity to Humidity. *Sci. Rep.* **2017**, *7*, 41640.
(36) Kim, K.-J.; Lu, P.; Culp, J. T.; Ohodnicki, P. R. Metal-Organic Framework Thin Film Coated Optical Fiber Sensors: A Novel Waveguide-Based Chemical Sensing Platform. *ACS Sensors* **2018**, *3* (2), 386−394.
(37) Chocarro-Ruiz, B.; Pérez-Carvajal, J.; Avci, C.; Calvo-Lozano, O.; Alonso, M. I.; Maspoch, D.; Lechuga, L. M. A CO 2 Optical Sensor Based on Self-Assembled Metal−organic Framework Nanoparticles. *J. Mater. Chem. A* **2018**, *6* (27), 13171−13177.
(38) Pang, S. H.; Han, C.; Sholl, D. S.; Jones, C. W.; Lively, R. P. Facet-Specific Stability of ZIF-8 in the Presence of Acid Gases Dissolved in Aqueous Solutions. *Chem. Mater.* **2016**, *28* (19), 6960−6967.
(39) Bhattacharyya, S.; Han, R.; Kim, W.-G.; Chiang, Y.; Jayachandrababu, K. C.; Hungerford, J. T.; Dutzer, M. R.; Ma, C.; Walton, K. S.; Sholl, D. S.; Nair, S. Acid Gas Stability of Zeolitic Imidazolate Frameworks: Generalized Kinetic and Thermodynamic Characteristics. *Chem. Mater.* **2018**, *30* (12), 4089−4101.
(40) Dutta, A.; Tymińska, N.; Zhu, G.; Collins, J.; Lively, R. P.; Schmidt, J. R.; Vasenkov, S. Influence of Hydrogen Sulfide Exposure on the Transport and Structural Properties of the Metal−Organic Framework ZIF-8. *J. Phys. Chem. C* **2018**, *122* (13), 7278−7287.
(41) Zhang, H.; Liu, D.; Yao, Y.; Zhang, B.; Lin, Y. S. Stability of ZIF-8 Membranes and Crystalline Powders in Water at Room Temperature. *J. Membr. Sci.* **2015**, *485*, 103−111.
(42) Tian, F.; Cerro, A. M.; Mosier, A. M.; Wayment-Steele, H. K.; Shine, R. S.; Park, A.; Webster, E. R.; Johnson, L. E.; Johal, M. S.; Benz, L. Surface and Stability Characterization of a Nanoporous ZIF-8 Thin Film. *J. Phys. Chem. C* **2014**, *118* (26), 14449−14456.
(43) Zhang, W.; Hu, Y.; Ge, J.; Jiang, H.; Yu, S.; Zhang, W.; Hu, Y.; Ge, J.; Jiang, H.; Yu, S. A Facile and General Coating Approach to Moisture/Water- Resistant Metal-Organic Frameworks with Intact Porosity A Facile and General Coating Approach to Moisture/Water-Resistant Metal-Organic Frameworks with Intact Porosity. *J. Am. Chem. Soc.* **2014**, *136*, 16978−16981.
(44) Park, K. S.; Ni, Z.; Cote, A. P.; Choi, J. Y.; Huang, R.; Uribe-Romo, F. J.; Chae, H. K.; O'Keeffe, M.; Yaghi, O. M. Exceptional Chemical and Thermal Stability of Zeolitic Imidazolate Frameworks. *Proc. Natl. Acad. Sci. U. S. A.* **2006**, *103* (27), 10186−10191.
(45) Kizzie, A. C.; Wong-foy, A. G.; Matzger, A. J. Effect of Humidity on the Performance of Microporous Coordination Polymers as Adsorbents for CO2 Capture. *Langmuir* **2011**, *27* (10), 6368−6373.
(46) Knoll, W. Interfaces and Thin Films as seen by bound Electromagnetic Waves. *Annu. Rev. Phys. Chem.* **1998**, *49* (1), 569−638.
(47) Ma, B. H.; Jen, A. K.; Dalton, L. R. Polymer-Based Optical Waveguides: Materials, Processing, and Devices. *Adv. Mater.* **2002**, *14*, 1339−1365.
(48) Hang, K.; Lau, A.; Tan, L.; Tamada, K.; Sander, M. S.; Knoll, W. Highly Sensitive Detection of Processes Occurring Inside Nanoporous Anodic Alumina Templates: A Waveguide Optical Study. *J. Phys. Chem. B* **2004**, *108* (30), 10812−10818.
(49) Cameron, P. J.; Jenkins, a. T. a.; Knoll, W.; Marken, F.; Milsom, E. V.; Williams, T. L. Optical Waveguide Spectroscopy Study of the Transport and Binding of Cytochrome c in Mesoporous Titanium Dioxide Electrodes. *J. Mater. Chem.* **2008**, *18* (36), 4304.

DOI: 10.1021/acs.jpca.8b09610
J. Phys. Chem. A 2019, 123, 1100−1109

(50) Kim, D. H.; Lau, K. H. A.; Robertson, J. W. F.; Lee, O.-J. J.; Jeong, U.; Lee, J. I.; Hawker, C. J.; Russell, T. P.; Kim, J. K.; Knoll, W. Thin Films of Block Copolymers as Planar Optical Waveguides. *Adv. Mater.* **2005**, *17* (20), 2442−2446.
(51) Kim, D. H.; Lau, K. H. A.; Joo, W.; Peng, J.; Jeong, U.; Hawker, C. J.; Kim, J. K.; Russell, T. P.; Knoll, W. An Optical Waveguide Study on the Nanopore Formation in Block Copolymer/Homopolymer Thin Films by Selective Solvent Swelling. *J. Phys. Chem. B* **2006**, *110* (31), 15381−15388.
(52) Lau, K. H. A.; Knoll, W.; Kim, D. H. Theoretical Optical Waveguide Investigation of Self-Organized Polymer Thin Film Nanostructures with Nanoparticle Incorporation Optical Waveguide Spectroscopy. *Macromol. Res.* **2007**, *15* (3), 211−215.
(53) Yang, X.; Lin, X.; Zhao, Y.; Zhao, Y. S.; Yan, D. Lanthanide Metal-Organic Framework Microrods: Colored Optical Waveguides and Chiral Polarized Emission. *Angew. Chem., Int. Ed.* **2017**, *56* (27), 7853−7857.
(54) Shekhah, O.; Liu, J.; Fischer, R. A.; Wöll, C. MOF Thin Films: Existing and Future Applications. *Chem. Soc. Rev.* **2011**, *40* (2), 1081.
(55) Hou, C.; Xu, Q.; Peng, J.; Ji, Z.; Hu, X. (110)-Oriented ZIF-8 Thin Films on ITO with Controllable Thickness. *ChemPhysChem* **2013**, *14* (1), 140−144.
(56) Zimpel, A.; Preiß, T.; Röder, R.; Engelke, H.; Ingrisch, M.; Peller, M.; Rädler, J. O.; Wagner, E.; Bein, T.; Lächelt, U.; Wuttke, S. Imparting Functionality to MOF Nanoparticles by External Surface Selective Covalent Attachment of Polymers. *Chem. Mater.* **2016**, *28* (10), 3318−3326.
(57) Tan, J.; Bennett, T. D.; Cheetham, A. K. Chemical Structure, Network Topology, and Porosity Effects on the Mechanical Properties of Zeolitic Imidazolate Frameworks. *Proc. Natl. Acad. Sci. U. S. A.* **2010**, *107* (22), 9938−9943.
(58) Tuninetti, J. S.; Rafti, M.; Azzaroni, O. Early Stages of ZIF-8 Film Growth: The Enhancement Effect of Primers Exposing Sulfonate Groups as Surface-Confined Nucleation Agents. *RSC Adv.* **2015**, *5* (90), 73958−73962.
(59) Rafti, M.; Allegretto, J. A.; Segovia, G. M.; Tuninetti, J. S.; Giussi, J. M.; Bindini, E.; Azzaroni, O. Metal−organic Frameworks Meet Polymer Brushes: Enhanced Crystalline Film Growth Induced by Macromolecular Primers. *Mater. Chem. Front.* **2017**, *1* (11), 2256−2260.
(60) Wang, H.; Jian, M.; Qi, Z.; Li, Y.; Liu, R.; Qu, J.; Zhang, X. Specific Anion Effects on the Stability of Zeolitic Imidazolate Framework-8 in Aqueous Solution. *Microporous Mesoporous Mater.* **2018**, *259*, 171−177.
(61) Zhang, L.; Hu, Y. H. Strong Effects of Higher-Valent Cations on the Structure of the Zeolitic Zn(2-Methylimidazole) $_2$ Framework (ZIF-8). *J. Phys. Chem. C* **2011**, *115* (16), 7967−7971.

DOI: 10.1021/acs.jpca.8b09610
J. Phys. Chem. A 2019, 123, 1100−1109